

# Preparation and characterization of ZnO/graphene nanocomposite for improved photovoltaic performance

P. Jayabal · S. Gayathri · V. Sasirekha ·  
J. Mayandi · V. Ramakrishnan

Received: 8 May 2014 / Accepted: 3 September 2014 / Published online: 11 October 2014  
© Springer Science+Business Media Dordrecht 2014

**Abstract** Zinc oxide (ZnO) nanoparticles and ZnO/graphene (ZG) nanocomposite were synthesized via simple chemical route and its application as a photoanode for dye-sensitized solar cell (DSSC) was demonstrated. The prepared ZnO and ZG were structurally characterized by X-ray diffraction and micro-Raman techniques. The scanning electron micrograph of ZG revealed the spherical-shaped ZnO nanoparticles of particle size  $\sim 160$  nm was anchored on the two-dimensional graphene sheets. UV-Vis absorption spectroscopy showed that the ZG nanocomposite has enriched visible light absorption. The DSSCs were fabricated using the synthesized ZnO

and ZG nanocomposite as photoanode and the effect of low-cost organic dyes on the photovoltaic performances of the solar cells were investigated. Comprehensive performances of ZG are better than that of ZnO-based DSSCs. The ZG DSSCs show power conversion efficiency (PCE) of 1.5 and 0.98 % for RB and EY sensitized electrodes, respectively. Moreover, the ZG dominates in many aspects due to the presence of graphene.

**Keywords** ZnO · Nanocomposite · Graphene · Micro-Raman · Solar cells · Energy conversion

## Introduction

Nanocomposites composed of two or more materials with desired performance are recently one of the most researched areas, mainly due to the synergic effect between the materials that are essential for technological applications in various areas (Xiang et al. 2012). Metal oxides and carbon allotropes are two of the most attractive materials in the materials science community. ZnO is the most investigated functional material in the family of metal oxides (Wahab et al. 2007; Marlinda et al. 2012). It is a II-VI compound semiconductor with a direct bandgap of 3.37 eV at room temperature. The superior properties such as anti-oxidation, large excitation binding energy (60 meV), higher electron mobility ( $115\text{--}155\text{ cm}^2\text{ V}^{-1}\text{ s}^{-1}$ ), and

---

P. Jayabal · S. Gayathri · V. Ramakrishnan  
Department of Laser Studies, School of Physics, Madurai  
Kamaraj University, Madurai 625021, India

V. Sasirekha  
Department of Physics, Avinashilingam University,  
Coimbatore 641 043, India

J. Mayandi  
Department of Materials Science, School of Chemistry,  
Madurai Kamaraj University, Madurai 625021, India

V. Ramakrishnan (✉)  
Indian Institute of Science Education and Research  
Thiruvananthapuram,  
Thiruvananthapuram 695 016, Kerala, India  
e-mail: vr.optics1@gmail.com

chemical stability of ZnO have great potential in the applications for optical detector, gas sensor, solar cell, short-wavelength UV laser, photocatalysts, microsensors and blue or green optoelectronic devices, and so on (Anta et al. 2012; Rani et al. 2008). One of the carbon allotropes, graphene is a two dimensional, one-atom-thick layer made of carbon atoms in a hexagonal lattice which has high carrier mobility, high thermal conductivity, electrical conductivity, and high surface area  $2,600 \text{ m}^2 \text{ g}^{-1}$  (theoretical prediction) (Marlinda et al. 2012; Dhar et al. 2013; Sahoo et al. 2014; Zhao et al. 2014). Therefore, ZnO–graphene nanocomposite (ZG) is expected to exhibit remarkable properties in the applications like solar energy conversion, energy storage, optoelectronic, and photocatalytic activity (Lightcap et al. 2013; Xiang et al. 2012; Marlinda et al. 2012).

Currently, ZnO–graphene nanocomposites (ZG) are attracting a great deal of attention due to their potential applications in recent research areas (Akhavan 2010; Chen et al. 2011; Cuong et al. 2010; Hwang et al. 2011). The dye-sensitized solar cells (DSSCs) are considered as prospective tools for their versatility such as low cost, convenient fabrication, industrial applications, and high power conversion efficiencies ( $>12\%$ ) (Gratzel and Hagfeldt 2000; Gratzel 2001, 2003, 2005). It has been shown that  $\text{TiO}_2$  combined with graphene shows enhanced photovoltaic performance. According to the reported literatures (Tang et al. 2010; Lightcap et al. 2013; Chen et al. 2013; Yang et al. 2010; Lee et al. 2012), the highly improved performance of the  $\text{TiO}_2$ /graphene nanocomposite can be attributed to the higher transfer rate of photo-generated electrons and suppressed recombination of the photo-induced electron–hole pairs. Therefore, we expect the same behavior for ZG nanocomposite DSSCs.

In this paper, a simple one-step chemical reduction route was proposed to prepare a ZG nanocomposite using graphene oxide (GO) and zinc acetate  $\text{Zn}(\text{Ac})_2 \cdot 2\text{H}_2\text{O}$  as source materials, and  $\text{N}_2\text{H}_4$  was used as reducing agent. The synthesized ZG nanocomposite was subjected to structural and optical characterizations. We have used the prepared ZG nanocomposite as a working electrode in DSSC. The DSSCs were made using low-cost organic dyes such as rose bengal (RB) and eosin yellow (EY) as sensitizer, and their photovoltaic performances have been studied.

## Experimental

### Materials

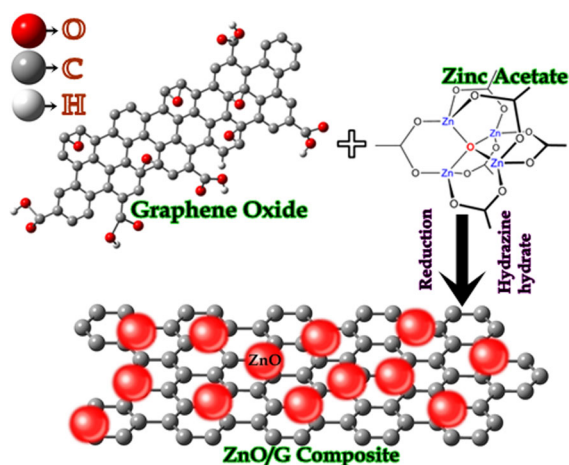
Zinc acetate dihydrate  $\text{Zn}(\text{Ac})_2 \cdot 2\text{H}_2\text{O}$  (Merck), glycerol (Sigma), rose bengal (RB, Alfa), eosin yellow (EY, Alfa), sodium hydroxide pellets (NaOH, Nice), graphite plate (Alfa), graphite powder (Alfa), 37 % hydrochloric acid (HCl, Merck), 98 % sulfuric acid ( $\text{H}_2\text{SO}_4$ , Merck), hydrogen peroxide ( $\text{H}_2\text{O}_2$ , Merck), potassium permanganate ( $\text{KMnO}_4$ , Merck), hydrazine hydrate ( $\text{N}_2\text{H}_4$ , Merck), ethylene glycol (EG, Merck), potassium iodide (KI, Merck), iodine (I, Merck), and absolute ethanol (Merck) were purchased and used as received without further purification.

### Synthesis of zinc oxide (ZnO)

ZnO nanoparticles were synthesized by directly mixing 1 g of  $\text{Zn}(\text{Ac})_2 \cdot 2\text{H}_2\text{O}$  in 100 ml of deionized water under stirring condition. Then, a corresponding amount of 1 M NaOH aqueous solution was added to the above solution and stirred for 3 h. The resultant precipitate was centrifuged and washed with deionized water. Later, the final product was dried at  $100^\circ\text{C}$  and the dried powder was annealed at  $450^\circ\text{C}$  for 4 h.

### Synthesis of ZG nanocomposite

GO was synthesized from graphite powder according to the improved Hummer's method (Hummers and



**Scheme 1** Schematic illustration of the formation of ZnO/graphene composite from graphene oxide

Offeman 1958). Initially, 900 mg of  $\text{Zn}(\text{Ac})_2 \cdot 2\text{H}_2\text{O}$  was added to 90 ml of GO ( $10 \text{ mg ml}^{-1}$ ) solution and stirred for 3 h. Then, appropriate amount of  $\text{N}_2\text{H}_4$  was added drop by drop to the above solution and the resulting mixture was stirred at  $80^\circ\text{C}$ . After 3 h, the brown color solution turned to black indicating the reduction of GO to graphene. At this stage, the stirring is stopped and the precipitate was collected by centrifugation and then washed using water and alcohol. Further, the obtained powder was dried at  $100^\circ\text{C}$  and then annealed at  $450^\circ\text{C}$  for 4 h in a muffle furnace. Schematic illustration of the formation of ZG nanocomposite from graphene oxide is shown in Scheme 1.

#### Preparation of electrodes and cell assembly

In the solar cell fabrication, synthesized ZnO and ZG powder were made into a paste by grinding powder in a mortar for about 30 min using glycerol as dispersing agent. Then, the paste was coated on the indium tin oxide (ITO) by doctor blade technique. In the electrode preparation, ITO substrate was covered with scotch tape 1 cm apart to control the thickness and area of the electrodes ( $1 \text{ cm} \times 1 \text{ cm}$ ). Then the prepared electrodes were annealed at  $300^\circ\text{C}$  for 1 h to evaporate the solvent. The photoanode was prepared by immersing the slightly warmed ZnO and ZG electrodes into the 0.5 mM of RB and EY dye solutions for 12 h. The non-adsorbed dye was washed up with acetonitrile. For the preparation of counter electrode, a piece of graphite plate was scratched uniformly on the ITO plate. The graphite coated ITO electrodes and dye-coated ZnO and ZG electrodes were placed facing each other and held together using the binder clips. The electrolyte solution was prepared by mixing 0.127 g of iodine and 0.83 g of potassium iodide (KI) in 10 ml of ethylene glycol. The iodide electrolyte solution was injected between the anode and cathode prior to the I–V measurement.

#### Dye desorption study

In order to analyze the amount of dye loading, the dye was desorbed completely from the dye-loaded electrodes. In the desorption study, the dye-anchored ZnO and ZG electrodes were immersed into the 0.1 mM NaOH in ethanol for about 12 h. Further, the desorbed solutions were taken in a 1-cm path length cuvette as

sample and NaOH solution as reference. A double beam UV–Vis spectrophotometer was used to measure the desorbed dye concentration.

#### Instrumentation

The structural analysis was carried out by powder PANalytical X-ray diffractometer with  $\text{CuK}\alpha$  radiation ( $\lambda = 1.54 \text{ \AA}$ ). The surface morphology and composition of the samples were examined by field emission scanning electron microscope (FE-SEM, FEI Nova 400 Nano SEM) equipped with the energy dispersive X-ray spectrometry (Bruker Quantax 200 AS). Raman-scattering measurements were performed in  $180^\circ$  backscattering geometry using a LabRamanHR800 spectrometer from Horiba Jobin–Yvon equipped with a CCD detector. The sample was excited by 633 nm emission from a He–Ne laser and the accuracy of the wavenumber was about  $0.3 \text{ cm}^{-1}$ . The absorbance spectra were measured using Shimadzu (UV2450) UV–Vis spectrophotometer. Oriel class-A solar simulator (91195A, Newport) was used as a light source, and a computer-controlled Autolab PGSTAT302N electrochemical workstation was employed for current–voltage (I–V) measurements.

#### Results and discussion

The X-ray diffraction pattern of ZnO and ZG is shown in Fig. 1. The diffraction peaks at  $31.8^\circ$ ,  $34.5^\circ$ ,  $36.3^\circ$ ,  $47.6^\circ$ ,  $56.6^\circ$ ,  $62.8^\circ$ ,  $68.1^\circ$ , and  $69.2^\circ$  correspond to the (100), (002), (101), (102), (110), (103), (112), and (201) planes, respectively, and can be indexed to wurtzite structure of ZnO. The observed planes are also consistent with the standard JCPDS data file (Card No. 89-0510). On the other hand, the ZG nanocomposite also exhibits the similar planes corresponding to the ZnO wurtzite structure. In addition to the ZnO diffraction peaks, the appearance of weak broad peak at  $25^\circ$  is attributed to the characteristic peak of graphene. The absence of peaks from graphene oxide indicated that the reduction of graphene oxide is complete in the synthesis process (Xu et al. 2008; Li et al. 2011) and confirms the formation of ZG nanocomposite.

The room temperature Raman spectra of ZnO and ZG excited at 633 nm are presented in Fig. 2. The ZnO exhibits hexagonal wurtzite structure which

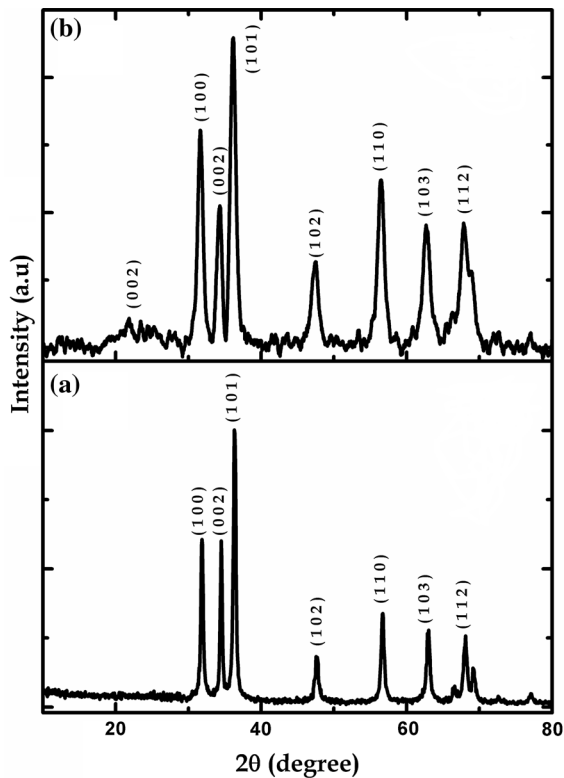


**Fig. 1** XRD pattern of the synthesized **a** ZnO nanoparticles and **b** ZG nanocomposite

belongs to the  $C_{6v}^4$  space group having two formula units per primitive cell with all the atoms occupying the  $C_{3v}$  sites. According to group theoretical analysis, the phonons of wurtzite structure ZnO have irreducible representation (Zeferino et al. 2011; Cheng et al. 2010).

$$\Gamma = A_1 + 2B_1 + E_1 + 2E_2,$$

where  $B_1$  modes are IR and Raman inactive, i.e., silent mode and  $E_2$  modes are Raman active. The Raman and IR active modes  $A_1$  and  $E_1$  are polar, and therefore, each splits into LO and TO modes. The foremost sharp peak at  $437\text{ cm}^{-1}$ ,  $E_2$  (high) mode, is the characteristic peak of hexagonal wurtzite phase ZnO and the peaks at  $\sim 98, 380, 407,$  and  $583\text{ cm}^{-1}$  correspond to  $E_2$  (low),  $A_1$  (LO),  $E_1$  (TO), and  $E_1$  (LO) modes, respectively. The second-order Raman scattering originating from the zone boundary phonons  $E_2(H)-E_2(L)$  give rise to a peak at  $\sim 338\text{ cm}^{-1}$ . The experimentally observed modes at  $328, 378, 432,$  and  $578\text{ cm}^{-1}$  for the ZnO sample show that there is no major shift from the typical vibrational modes of wurtzite phase, which

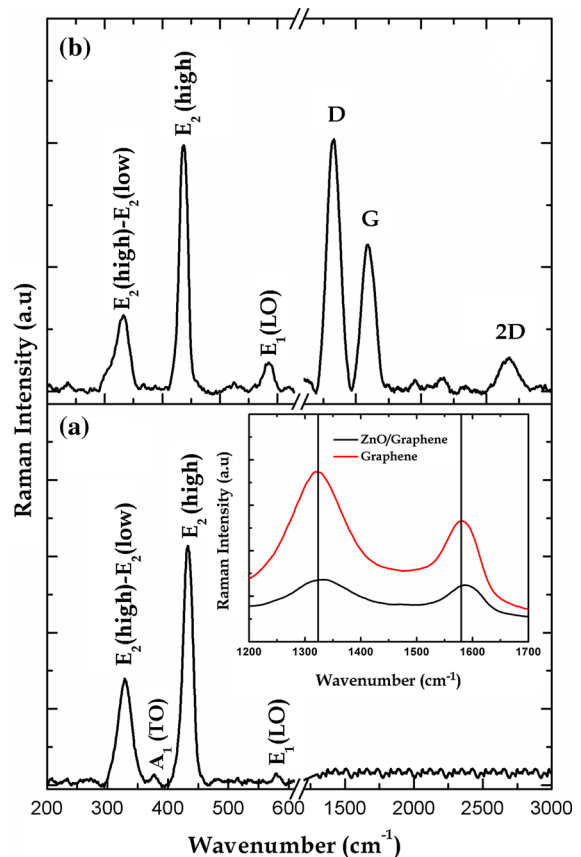


**Fig. 2** Micro-Raman spectra of synthesized **a** ZnO nanoparticles and **b** ZG nanocomposite excited by (He-Ne) 633 nm laser line (*inset*) D and G band of graphene and ZG nanocomposite

confirms the existing phase was purely of wurtzite type. Furthermore, the ZG sample shows the main characteristic peak of hexagonal wurtzite ZnO at  $436\text{ cm}^{-1}$  corresponding to the vibration mode of  $E_2$  phonon was observed, and low-intensity peak at  $332\text{ cm}^{-1}$  was caused by the multiple-phonon scattering processes of ZnO (Cheng et al. 2010). In addition, the peaks at  $1,330, 1,592,$  and  $2,674\text{ cm}^{-1}$  are also observed, which indicate that the graphene was preserved. The Raman active modes at  $1,330$  (D band) and  $1,592\text{ cm}^{-1}$  (G band) correspond to breathing mode of  $\kappa$ -point phonons of  $A_{1g}$  symmetry and the  $E_{2g}$  phonon of  $sp^2$  C atoms, respectively, and the second-order of zone boundary phonons gives rise to 2D ( $2,674\text{ cm}^{-1}$ ) band. The D band of graphene is more intense than the G band, where the higher intensity of D band reflects the prepared sample have more defects due to the incorporation of ZnO in graphene (Omar

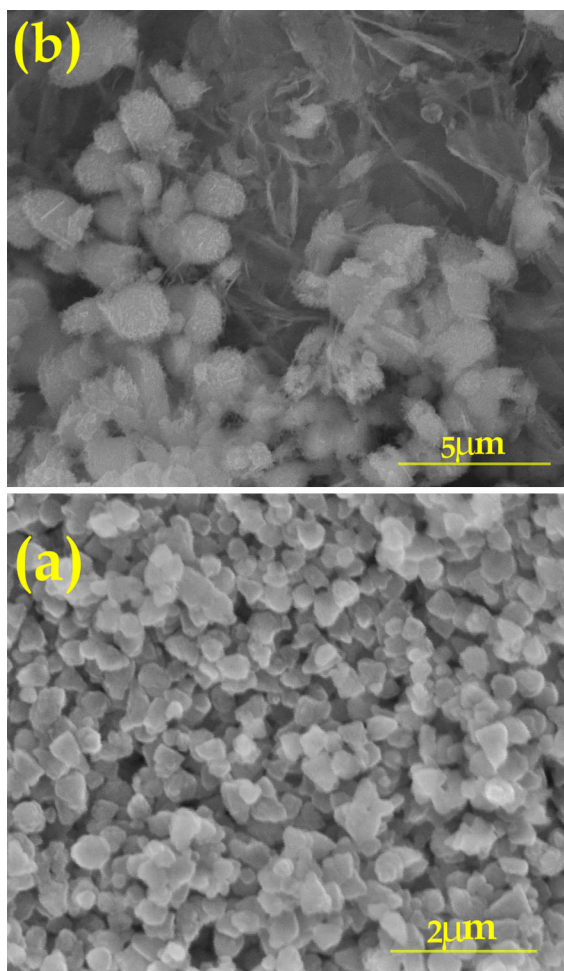


**Fig. 3** FE-SEM images of **a** ZnO nanoparticles and **b** ZG nanocomposite

et al. 2014; Xu et al. 2011) and also the G band of ZG nanocomposite was shifted about  $10\text{ cm}^{-1}$  toward the higher wavenumber region compared with graphene indicating the chemical interaction between graphene and ZnO (Fig. 2 (inset)) (Lv et al. 2014; Xu et al. 2011; Kamat 2010). The Raman spectrum showed ZnO vibrations as well as D, G, and 2D bands of graphene, suggesting that the structure of ZnO and graphene is retained in the ZG nanocomposite (Chen et al. 2011; Luo et al. 2012; Nayak et al. 2013) and the observed Raman results are in accordance with the XRD results.

Figure 3 depicts the FE-SEM images of ZnO and ZG nanocomposite. From the Fig. 3a, it is clear that the spherical-shaped ZnO nanoparticles are uniformly distributed and the particles are very closely packed and make the surface denser. The statistical average

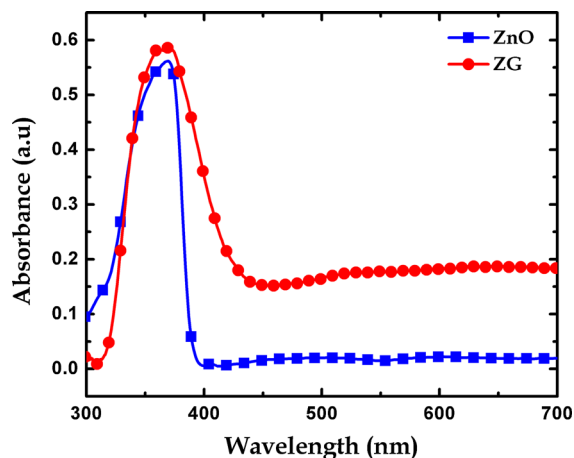


**Fig. 4** UV-Vis absorption spectra of ZnO and ZG electrodes

size of the particles is estimated as  $\sim 320\text{ nm}$ . In the case of Fig. 3b, there are two different morphologies, including nanoparticles from ZnO and wrinkled sheet-like morphology from graphene indicates ZnO nanoparticles are well anchored on the surface of the graphene sheets. The size of ZnO particles in ZG nanocomposite is  $\sim 160\text{ nm}$  which was distributed randomly on the graphene layer and the existence of ZnO is favorable to prevent the graphene from aggregation. Hence, the SEM image of ZG adds evidence for the formation of nanocomposite.

As the results of XRD, Raman and FE-SEM confirmed the formation of ZnO nanoparticles and ZG nanocomposite and clarified the structural characteristics of ZnO and graphene is not affected during the synthesis of ZG nanocomposite. The ZnO nanoparticle and ZG nanocomposite electrodes were prepared as discussed in experimental part. The UV-Vis absorption spectra of ZnO and ZG films are shown in Fig. 4. The absorption band at 370 nm for ZnO film, which originates from the band gap transitions confirmed the existence of highly crystalline ZnO (Zhang et al. 2009a). In the case of ZG nanocomposite, the absorbance has increased in the entire region and the absorption edge shifted toward higher wavelength region (red shift) due to the incorporation of graphene. The bandgap energy of graphene incorporated ZnO is lower (2.78 eV) than bare ZnO (3.19 eV). Therefore, this result indicated that narrowing of the band gap of ZnO occurred with the addition of graphene. The reduction in bandgap of ZnO with the addition of



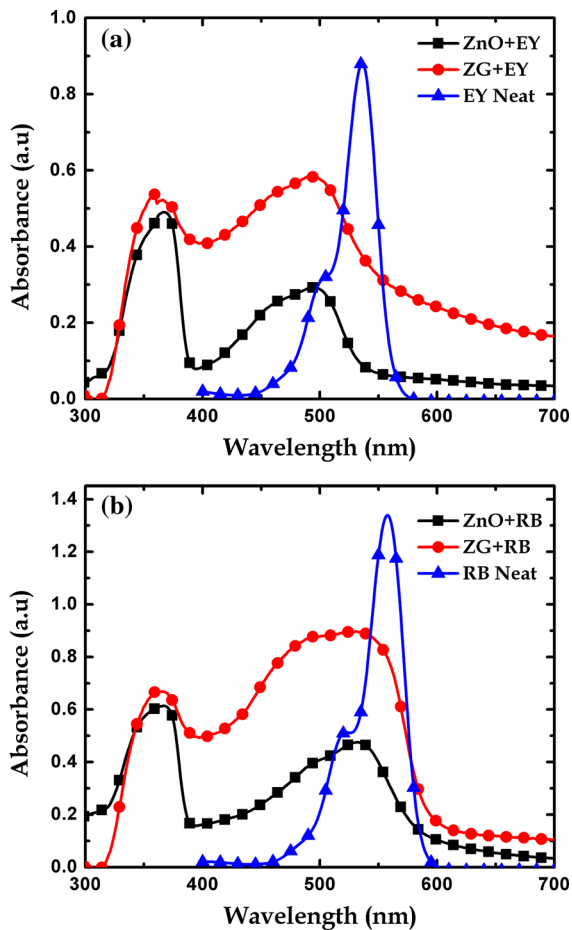


**Fig. 5** UV-Vis absorption spectra of **a** EY, EY sensitized ZnO and ZG electrodes and **b** RB, RB sensitized ZnO and ZG electrodes

graphene might be attributed to the chemical interaction between ZnO and graphene (Zhang et al. 2010a, b). The analysis of the obtained results suggests that the presence of graphene can tune the optical properties of ZnO (Zhang et al. 2009b; Liu et al. 2011).

Figure 5 shows UV-Vis absorption spectra of (a) EY, EY sensitized ZnO and ZG electrodes and (b) RB, RB sensitized ZnO and ZG electrodes. The RB and EY dyes are xanthene sensitizers with high absorption coefficient in the visible region and have absorption in the visible region with maximum absorbance at 556 and 535 nm, respectively, and satisfy the major condition for their use as sensitizers in DSSCs (Chen et al. 2007). The dye-anchored ZnO electrodes show an absorption band in the UV region corresponding to the band to band transition of ZnO,

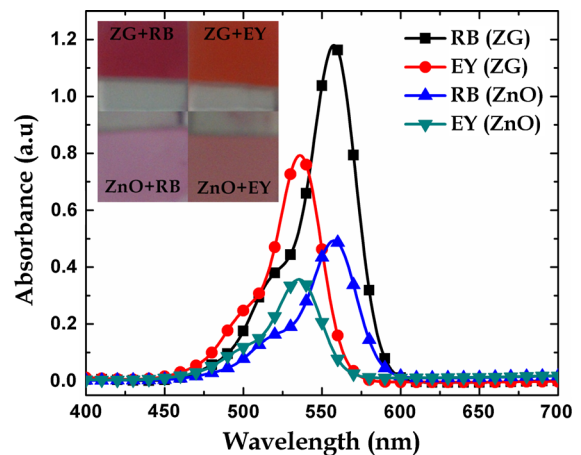


**Fig. 6** UV-Vis absorbance spectra of dyes desorbed from ZnO electrodes, ZG electrodes, and (inset) digital images of dye-anchored ZnO and ZG electrodes

whereas other bands observed at 558 and 537 nm originate from the dye molecules adsorbed on the ZnO surface. Therefore, it is clearly evident that, the dye molecules are loaded on ZnO electrodes and they enable ZnO to absorb visible light. On the other hand, ZG electrodes also show UV absorption around 365 nm as well as a broad visible absorption band. The absorption bands of ZG and dye-anchored ZG get broadened with higher absorption intensities in the visible region compared with bare ZnO due to the addition of graphene. Hence, the improvement of absorbed photon energy toward the visible region is expected to enhance the photoconductivity of ZG compared with bare ZnO. Further, it can be observed that the absorption peaks of dyes anchored on the ZnO and ZG electrodes are broadened and blue-shifted compared to the spectra of neat dye solutions. This is hence an indication that the anchoring of dyes is via chemical interactions to the ZnO and ZG surface (Moser and Gratzel 1984; Hagfeldt et al. 2010).

To support the effective adsorption of dyes used in our study, we also investigated the absorption spectra of desorbed dyes from ZnO and ZG electrodes, and the spectra are presented in Fig. 6. From the absorbance spectra, the dye desorbed from the ZG electrodes show higher absorption intensity than ZnO electrodes, which confirms the higher dye anchoring capability of ZG electrodes. Also, the naked eye inspection (photographs) provides a clear view of better dye adsorption of ZG electrodes than ZnO electrodes, which is shown in Fig. 6 (inset). It is found that more

**Table 1** Photovoltaic parameters of DSSCs based on ZnO and ZG nanocomposite

S. no.	Photoanode	Adsorbed dye (mol cm <sup>-2</sup> )	J <sub>sc</sub> (A cm <sup>-2</sup> )	V <sub>oc</sub> (V)	FF (%)	η (%)
1.	ZnO+RB	5.4 × 10 <sup>-6</sup>	0.00128	0.65	0.51	1.04
2.	ZnO+EY	3.2 × 10 <sup>-6</sup>	0.00092	0.67	0.48	0.66
3.	ZG+RB	1.3 × 10 <sup>-5</sup>	0.00160	0.70	0.53	1.50
4.	ZG+EY	7.1 × 10 <sup>-6</sup>	0.00110	0.69	0.51	0.98

number of dye molecules are attached to the surface of the ZG electrodes, which might be due to the high surface area of graphene and chemical interaction between the dye molecules and graphene (Shahzad et al. 2013). It is suggested that the enhancement of dye adsorption in ZG electrodes is not only due to simple physisorption but also attributed to the π-π stacking interaction between the dye molecule and the aromatic domains of graphene (Grätzel 2005; Shahzad et al. 2013). The amount of adsorbed dye is calculated using Beer’s law and is presented in Table 1.

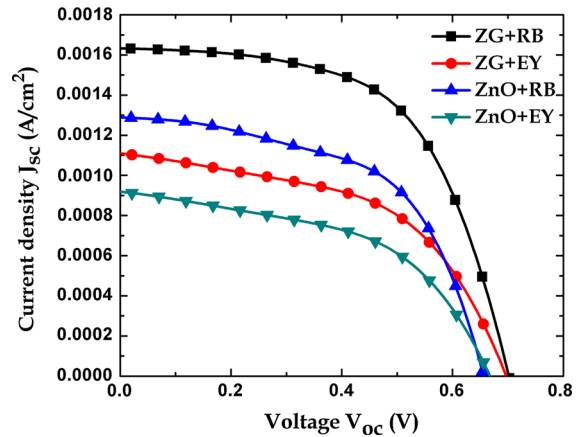
The photovoltaic examination of DSSCs made with ZnO and ZG electrodes was carried out by measuring the current–voltage (I–V) characteristic curves using an electrochemical workstation under irradiation of artificial sunlight from 100 W xenon arc lamp with incident light intensity of 40 mW cm<sup>-2</sup> (AM 1.5). The photovoltaic performances such as fill factor (FF) and PCE (η) of DSSCs were calculated according to the following equations:

$$FF = V_m J_m / V_{oc} J_{sc} \tag{1}$$

$$\eta = V_{oc} J_{sc} FF / P_{in}, \tag{2}$$

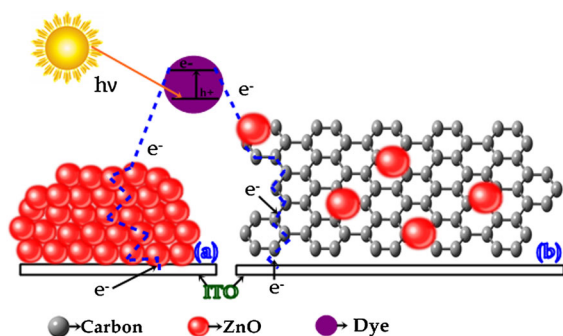
where V<sub>oc</sub> is the open-circuit voltage (V), J<sub>sc</sub> the short-circuit current density (mA cm<sup>-2</sup>), and V<sub>m</sub> (V) and J<sub>m</sub> (mA cm<sup>-2</sup>) the voltage and the current density at the point of maximum power output in the current density–voltage (J–V) plot, respectively, and P<sub>in</sub> is the incident light power (Nazeeruddin et al. 2011). The obtained parameters of DSSCs such as J<sub>sc</sub>, V<sub>oc</sub>, FF, and PCE calculated from the J–V curves are summarized in Table 1.

Figure 7 depicts the J–V characteristic curves of ZnO and ZG-based DSSCs. From the observed results, it is evident that the photovoltaic performance of ZG is better than the bare ZnO-based DSSCs. The enhancement of parameters such as PCE, V<sub>oc</sub>, J<sub>sc</sub>, and FF was influenced by two factors such as higher dye loading of ZG electrodes and anti-recombination effect of



**Fig. 7** J–V characteristics of DSSCs fabricated using ZnO and ZG electrodes

graphene. In ZG nanocomposite, ZnO is a good electron donor material and graphene is a relatively good electron acceptor material, so the interaction between these two materials provides better electron transport. Briefly, the 2D graphene bridges behave as an electron transfer channel due to its higher electron conduction (Kongkanand et al. 2007). Under light irradiation, the conduction band of ZnO receives electrons from HOMO level of dye molecule. As the ZnO nanoparticles are anchored on graphene, the excited electrons are captured without any hindrance. The collected electrons can be transported from ZnO to the conductive substrate efficiently through graphene bridges and hence the recombination was suppressed (Chen et al. 2013; Omar et al. 2013). The scheme of the electron transfer process in (a) ZnO DSSC and (b) ZG DSSC is shown in Scheme 2. Furthermore, the high optical transparency of graphene allows more sunlight to the dye molecules and enhances the light harvesting in the DSSCs. Moreover, the results showed that the maximum part of the solar light is unused in the ZnO-based DSSCs conversion



**Scheme 2** Electron transfer mechanism in the DSSCs made with **a** ZnO electrode and **b** ZG electrode

process because the dyes which we have used have sharp absorption bands in the visible region, so they convert photons only below 600 nm. Whereas in ZG-based DSSCs, the broad absorption behavior was observed due to the incorporation of graphene. This enhances the photoconductivity leading to higher PCE. Further investigations are in progress, to realize the importance of graphene incorporation with different proportions and to determine the enhancement in the photovoltaic efficiency and performance of ZG composites.

## Conclusions

The ZnO nanoparticles and ZG nanocomposite were successfully prepared by chemical reduction route. The (002) plane along with ZnO diffraction peaks in the XRD pattern indicated the presence of both ZnO and graphene in the nanocomposite. Similarly, in the micro-Raman spectrum, the presence of ZnO as well as graphene vibrational modes confirmed the formation of nanocomposite. The morphology of the synthesized composite indicates that the ZnO nanoparticles were embedded on the wrinkled graphene sheets. The optical absorbance of the ZG nanocomposite was enhanced in the visible region compared to bare ZnO. This was caused by the chemical interaction between ZnO and graphene that might have led to the creation of electron-hole pairs during light radiation. The presence of graphene in ZnO suppressed the electron-hole recombination and increased the efficiency of the cells. The ZG nanocomposite possessed great dye adsorption behavior, extended visible light

absorption, enhanced charge transport, and power conversion efficiencies simultaneously.

**Acknowledgments** This work was financially supported by DST-PURSE Programme of Madurai Kamaraj University. The authors thank DST-FIST for providing Powder XRD facility, UGC-UPE for providing micro-Raman and solar simulator facilities. The authors PJ & JM acknowledge Mr. Suresh, School of Energy Science, Madurai Kamaraj University for his assistance in I-V measurement.

## References

- Akhavan O (2010) Graphene nanomesh by ZnO nanorod photocatalysts. *ACS Nano* 4:4174–4180
- Anta JA, Guillen E, Zaera RT (2012) ZnO-based dye-sensitized solar cells. *J Phys Chem C* 116:11413–11425
- Chen Z, Li F, Huang C (2007) Organic D- $\pi$ -A dyes for dye sensitized solar cell. *Curr Org Chem* 11:1241–1258
- Chen YL, Hu ZA, Chang YQ, Wang HW, Zhang ZY, Yang YY, Wu HY (2011) Zinc oxide/reduced graphene oxide composites and electrochemical capacitance enhanced by homogeneous incorporation of reduced graphene oxide sheets in zinc oxide matrix. *J Phys Chem C* 115:2563–2571
- Chen L, Zhou Y, Tu W, Li Z, Bao C, Dai H, Yu T, Liu J, Zou Z (2013) Enhanced photovoltaic performance of a dye-sensitized solar cell using graphene-TiO<sub>2</sub> photoanode prepared by a novel in situ simultaneous reduction-hydrolysis technique. *Nanoscale* 5:3481–3485
- Cheng B, Sun W, Jiao J, Tian B, Xiao Y, Lei S (2010) Disorder-induced Raman scattering effects in one-dimensional ZnO nanostructures by incorporation and anisotropic distribution of Dy and Li codopants. *J Raman Spectrosc* 41:1221–1226
- Cuong TV, Phama VH, Chung JS, Shina EW, Yoo DH, Hahn SH, Huh JS, Rue GH, Kima EJ, Hur SH, Kohl PA (2010) Solution-processed ZnO-chemically converted graphene gas sensor. *Mater Lett* 64:2479–2482
- Dhar P, Ansari MHD, Gupta SS, Siva VM, Pradeep T, Patamatta A, Das SK (2013) Percolation network dynamicity and sheet dynamics governed viscous behavior of poly-dispersed graphene nanosheet suspensions. *J Nanopart Res* 15:2095/1–2095/12
- Gratzel M (2001) Molecular photovoltaics that mimic photosynthesis. *Pure Appl Chem* 73:459–467
- Gratzel M (2003) Dye-sensitized solar cells. *J Photochem Photobiol C Photochem Rev* 4:145–153
- Gratzel M (2005) Solar energy conversion by dye-sensitized photovoltaic cells. *Inorg Chem* 44:6841–6851
- Gratzel M, Hagfeldt A (2000) Molecular photovoltaics. *Acc Chem Res* 33:269–277
- Hagfeldt A, Boschloo G, Sun L, Kloo L, Pettersson H (2010) Dye-sensitized solar cells. *Chem Rev* 110:6595–6663
- Hummers WS, Offeman RE (1958) Preparation of graphene oxide. *Chem Soc* 80:1339
- Hwang JO, Lee DH, Kim JY, Han TH, Kim BH, Park M, No K, Kim SO (2011) Vertical ZnO nanowires/graphene hybrids



- for transparent and flexible field emission. *J Mater Chem* 21:3432–3437
- Kamat PV (2010) Graphene-based nanoarchitectures. Anchoring semiconductor and metal nanoparticles on a two-dimensional carbon support. *J Phys Chem Lett* 1:520–527
- Kongkanand A, Dominguez RM, Kamat PV (2007) Single wall carbon nanotube scaffolds for photoelectrochemical solar cells. Capture and transport of photogenerated electrons. *Nano Lett* 7:676–680
- Lee JS, You KH, Park CB (2012) Highly photoactive, low bandgap TiO<sub>2</sub> nanoparticles wrapped by graphene. *Adv Mater* 24:1084–1088
- Li B, Cao H (2011) ZnO@graphene composite with enhanced performance for the removal of dye from water. *J Mater Chem* 21:3346–3349
- Lightcap IV, Kamat PV (2013) Graphitic design: prospects of graphene-based nanocomposites for solar energy conversion, storage, and sensing. *Acc Chem Res* 46:2235–2243
- Liu X, Pan L, Lv T, Lu T, Zhu G, Sun Z, Sun C (2011) Microwave-assisted synthesis of ZnO–graphene composite for photocatalytic reduction of Cr(VI). *Catal Sci Technol* 1:1189–1193
- Luo QP, Yu XY, Lei BX, Chen HY, Kuang DB, Su CY (2012) Reduced graphene oxide-hierarchical ZnO hollow sphere composites with enhanced photocurrent and photocatalytic activity. *J Phys Chem C* 116:8111–8117
- Lv R, Wang X, Lv W, Xu Y, Ge Y, He H, Li G, Wu X, Li X, Li Q (2014) Facile synthesis of ZnO nanorods grown on graphene sheets and its enhanced photocatalytic efficiency. *J Chem Technol Biotechnol*. doi:10.1002/jctb.4347
- Marlinda AR, Huang NM, Muhamad MR, Anamt MN, Chang BYS, Yusoff N, Harrison I, Lim HN, Chia CH, Kumar SV (2012) Highly efficient preparation of ZnO nanorods decorated reduced graphene oxide nanocomposites. *Mater Lett* 80:9–12
- Moser J, Gratzel M (1984) Photosensitized electron injection in colloidal semiconductors. *J Am Chem Soc* 106:6557–6564
- Nayak P, Anbarasan B, Ramaprabhu S (2013) Fabrication of organophosphorus biosensor using ZnO nanoparticle-decorated carbon nanotube-graphene hybrid composite prepared by a novel green technique. *J Phys Chem C* 117:13202–13209
- Nazeeruddin Md K, Baranoff E, Gratzel M (2011) Dye-sensitized solar cells: a brief overview. *Sol Energy* 85:1172–1178
- Omar A, Abdullah H, Yarmo MA, Shaari S, Taha (2013) Morphological and electron transport studies in ZnO dye-sensitized solar cells incorporating multi- and single-walled carbon nanotubes. *J Phys D Appl Phys* 46:165503/1–165503/8
- Omar FS, Ming HN, Hafiz SM, Ngee LH (2014) Microwave synthesis of zinc oxide/reduced graphene oxide hybrid for adsorption-photocatalysis application. *Int J Photoenergy* 2014:1–8
- Rani S, Suri P, Shishodia PK, Mehra RM (2008) Synthesis of nanocrystalline ZnO powder via sol–gel route for dye-sensitized solar cells. *Sol Energy Mater Sol C* 92:1639–1645
- Sahoo AK, Srivastava SK, Raul PK, Gupta AK, Shrivastava R (2014) Graphene nanocomposites of CdS and ZnS in effective water purification. *J Nanopart Res* 16:2473/1–2473/17
- Shahzad N, Pugliese D, Lamberti A, Sacco A, Virga A, Gazia R, Bianco S, Shahzad MI, Tresso E, Pirri CF (2013) Monitoring the dye impregnation time of nanostructured photoanodes for dye sensitized solar cells. *J Phys Conf Ser* 439:012012/1–012012/12
- Tang YB, Lee CS, Xu J, Liu ZT, Chen ZH, He Z, Cao YL, Yuan G, Song H, Chen L, Luo L, Cheng HM, Zhang WJ, Bello I, Lee ST (2010) Incorporation of graphenes in nanostructured TiO<sub>2</sub> films via molecular grafting for dye-sensitized solar cell application. *ACS Nano* 4:3482–3488
- Wahab R, Ansari SG, Kim YS, Seo HK, Shin HS (2007) Room temperature synthesis of needle-shaped ZnO nanorods via sonochemical method. *App Surf Sci* 253:7622–7626
- Xiang Q, Yu J, Jaroniec M (2012) Graphene-based semiconductor photocatalysts. *Chem Soc Rev* 41:782–796
- Xu C, Wang X, Zhu J (2008) Graphene–metal particle nanocomposites. *J Phys Chem C* 112:19841–19845
- Xu T, Zhang L, Cheng H, Zhu Y (2011) Significantly enhanced photocatalytic performance of ZnO via graphene hybridization and the mechanism study. *App Catal B* 101:382–387
- Yang N, Zhai J, Wang D, Chen Y, Jiang L (2010) Two-dimensional graphene bridges enhanced photoinduced charge transport in dye-sensitized solar cells. *ACS Nano* 4:887–894
- Zeferino RS, Flores MB, Pal U (2011) Photoluminescence and Raman scattering in Ag-doped ZnO nanoparticles. *J Appl Phys* 109:014308/1–014308/6
- Zhang L, Cheng H, Zong R, Zhu Y (2009a) Photocorrosion suppression of ZnO nanoparticles via hybridization with graphite-like carbon and enhanced photocatalytic activity. *J Phys Chem C* 113:2368–2374
- Zhang Q, Dandeneau CS, Zhou X, Cao G (2009b) ZnO nanostructures for dye-sensitized solar cells. *Adv Mater* 21:4087–4108
- Zhang H, Lv X, Li Y, Wang Y, Li J (2010a) P25-graphene composite as a high performance photocatalyst. *ACS Nano* 4:380–386
- Zhang Y, Tang ZR, Fu X, Xu YJ (2010b) TiO<sub>2</sub>–graphene nanocomposites for gas phase photocatalytic degradation of volatile aromatic pollutant: is TiO<sub>2</sub>–graphene truly different from other TiO<sub>2</sub>–carbon composite materials? *ACS Nano* 4:7303–7314
- Zhao N, Cheng X, Zhou Y, Yang M, Yang J, Zhong T, Zheng S (2014) Synthesis of flexible free-standing silver nanoparticles–graphene films and their surface-enhanced Raman scattering activity. *J Nanopart Res* 16:2335/1–2335/11